Ocean Dynamics (2026) 76:67
https://doi.org/10.1007/s10236-026-01823-6

Influence of the Kuroshio intrusion into the South China Sea on the sea surface temperature cooling induced by tropical cyclones

Shukui Cheng[1] · Anzhou Cao[1] · Jinbao Song[1] · Xinyu Guo[2]

Received: 9 September 2025 / Accepted: 25 June 2026

Abstract

This study examines the influence of the Kuroshio intrusion into the South China Sea (SCS) on the sea surface temperature cooling (SSTC) induced by tropical cyclones (TCs) through numerical simulations. Two types of the Kuroshio intrusion are investigated, i.e. the looping path characterized by the formation of an anticyclonic eddy in the SCS, and the leaping path characterized by the minimal intrusion into the SCS. For comparison, a no-Kuroshio case with initial horizontally homogeneous stratification is also simulated. Results indicate that both the looping and leaping Kuroshio modify TC-induced SSTC compared to the no-Kuroshio case, through distinct mechanisms. The looping Kuroshio suppresses TC-induced SSTC to both sides of the Luzon Strait (LS). In the anticyclonic eddy induced by the looping Kuroshio to the west side of the LS, the suppression is related to the warmer subsurface water, smaller vertical temperature gradient and larger mixed layer depth, which lead to weaker vertical mixing. Whereas to the east side of the LS, the cause is horizontal advection. The leaping Kuroshio also suppresses TC-induced SSTC to the east side of the LS through strong horizontal advection, but it enhances the SSTC to the west side of the LS through enhanced vertical mixing. Moreover, it is found that TC-induced SSTC spreads downstream along the major axis of the leaping Kuroshio, which is caused by vertical mixing rather than horizontal advection.

Keywords Kuroshio intrusion · Tropical cyclone · Sea surface temperature cooling · Numerical simulation · South China Sea

1 Introduction

Tropical cyclones (TCs) are intense meteorological systems that occur over tropical and subtropical oceans, particularly in the Northwestern Pacific Ocean (D'Asaro et al., 2011). In recent decades, TCs have exhibited an increasing trend in both frequency and intensity, raising significant scientific and societal concerns (e.g., Mei and Xie 2016; Tan et al. 2023).

During the formation and development of a TC, the sea surface temperature (SST) plays an important role. On one hand, the formation and maintenance of a TC depend on the continuous transport of vapor and heat from the upper ocean to the atmosphere, which requires the SST to be larger than a certain threshold (Dare and McBride 2011; Tory and Dare 2015). On the other hand, a TC can cause pronounced SST cooling (SSTC) along its track, due to a combined effect of Ekman pumping, turbulent mixing and other processes (e.g. Jullien et al. 2012; Vincent 2012a, b; Zhang et al. 2021). Consequently, TC-induced SSTC exerts a negative feedback on the TC intensification (Schade and Emanuel 1999; Emanuel et al. 2004; Zhu and Zhang 2006; Wu et al. 2008). Therefore, understanding the mechanism through which a TC causes SSTC is of great importance, and it is also beneficial for the prediction of TC's further evolution.

Previous studies have revealed several mechanisms for TC-induced SSTC, among which vertical mixing and upwelling are two important ones. Intense vertical mixing driven by wind stress-induced vertical shear instability is

Responsible Editor: Jia Wang

✉ Anzhou Cao
caoanzhou@zju.edu.cn

[1] State Key Laboratory of Ocean Sensing & Ocean College, Zhejiang University, Zhoushan, China

[2] Center for Marine Environmental Studies, Ehime University, Matsuyama, Japan

Published online: 03 July 2026

the primary driver of SSTC, accounting for over 70% of the SSTC (Price 1981; Greatbatch 1984; Shay et al. 1992; Jacob et al. 2000; Jullien et al. 2012; Qiao et al. 2022). Upwelling, which is induced by Ekman pumping, transports colder water from the deep ocean upward, also contributing to the SSTC. Although upwelling contributes less to the SSTC than vertical mixing, it modulates the temperature gradient in the upper ocean, thereby affecting vertical mixing (Price 1981; Chiang et al. 2011; Jullien et al. 2012). Moreover, TC-induced SSTC is influenced by the ocean conditions, such as the mixed layer depth (MLD), temperature structure and stratification (Vincent et al. 2012a, b; Wei et al. 2017; Jiang et al. 2018; Cui et al. 2023; Cheng et al. 2024).

Previous studies also indicated that the multiscale ocean dynamical processes can modulate TC-induced SSTC. Lin et al. (2005) found that an anticyclonic eddy reduced TC-induced SSTC due to a thicker upper-ocean mixed layer, which inhibited the entrainment of colder deep water. Wu et al. (2007) further pointed out that the thicker mixed layer in the anticyclonic eddy restricted the SSTC in the TC center, whereas the higher SST in the anticyclonic eddy led to stronger SSTC in the trailed right-hand side wake region of the TC. Zheng et al. (2010) showed that preexisting cyclonic eddies enhanced TC-induced SSTC by a factor of 2, compared to a case without the eddies. Jaimes and Shay (2010) found that an anticyclonic eddy reduced TC-induced SSTC whereas a cyclonic eddy enhanced it, and they attributed these phenomena to the different evolution characteristics of TC-induced near-inertial waves in the anticyclonic and cyclonic eddies. Ma et al. (2018) revealed that a cyclonic eddy extended the occurrence and recovery time of TC-induced SSTC, whereas an anticyclonic eddy showed little influence. In addition to mesoscale eddies, internal tides are also found to be able to modulate TC-induced SSTC. Through a series of idealized experiments in the South China Sea (SCS), Cheng et al. (2023) showed that internal tides can enhance TC-induced SSTC by 0.2–0.4 °C in the Luzon Strait (LS). Guan et al. (2024) reported that internal tides-enhanced SSTC further suppressed the TC intensification in the SCS.

As the west boundary current in the Northwestern Pacific Ocean, the Kuroshio carries the Northwestern Pacific Ocean water characterized by high temperature and high salinity (Nitani 1975; Deser et al. 1996; Tseng et al. 2000). The Kuroshio influences the local ocean conditions of the SCS and East China Sea (Qu et al. 2000; Chen et al. 2009; Nan et al. 2011, 2015; Chou et al. 2013), and may hence affect TC-induced SSTC in these regions. However, the understanding of the Kuroshio's influence on TC-induced SSTC remains limited. First, the current understanding of the Kuroshio's influence on TC-induced SSTC remains debated. For example, Wu et al. (2008), Liu and Wei (2015) and He et al. (2022) reported that the Kuroshio weakens TC-induced SSTC and shortens the recovery time of cooling through continuous horizontal advection of warm water. Furthermore, He et al. (2022) noted that the Kuroshio's thicker warm water layer can suppress vertical mixing, thereby further reducing SSTC. In contrast, Wei et al. (2014) argued that the Kuroshio intensifies TC-induced SSTC, as its baroclinic potential energy can enhance vertical mixing. Second, the Kuroshio intrudes into the SCS near the LS via three distinct paths, i.e. the leaping, looping and leaking paths (Nan et al. 2011, 2015). These paths exhibit seasonal variability and differently influence the local temperature, salinity and circulation structure, thereby differently modulating TC-induced SSTC. Figure 1 shows the satellite-observed SSTC induced by TCs Hato (2017) and Hagupit (2008), which had similar tracks and passed over the LS in August and September, respectively. Because the Kuroshio took different paths during the two TCs (Fig. 1b and d), the SSTC patterns show large difference (Fig. 1a and c). Given that previous studies have primarily focused on the Kuroshio's influence on TC-induced SSTC in the East China Sea (Wu et al. 2008; Wei et al. 2014; Liu and Wei 2015; He et al. 2022), how different Kuroshio paths affect TC-induced SSTC in the SCS remains unclear. Hence, it is necessary to explore the influence of different Kuroshio intrusion types on TC-induced SSTC near the LS, as there are approximately 6 TCs passing over the LS annually (Xu et al. 2020).

The remainder of this paper is organized as follows. Section 2 introduces the numerical model configurations and data processing methodology. Section 3 presents the main results, including the validation of simulated results, TC-induced SSTC features under the influences of different Kuroshio intrusion types, as well as the analysis results of temperature equation in the mixed layer. A discussion is presented in Sect. 4. Finally, Sect. 5 summarizes this study.

2 Data and methods

2.1 Model configurations

The Coastal and Regional Ocean Community model (CROCO v1.1; https://www.croco-ocean.org) is used to simulate TC-induced SSTC under different Kuroshio intrusion types near the LS. Considering that the real case is very complicated, i.e., a TC can intensify itself when passing over the Kuroshio (Yu et al. 2020), and this process may vary among different TC cases, semi-idealized experiments are conducted in this study. In the semi-idealized experiments, the background currents (including the Kuroshio) are real, whereas the TC is idealized and its characteristics remain invariant during the simulation. In other words, this study

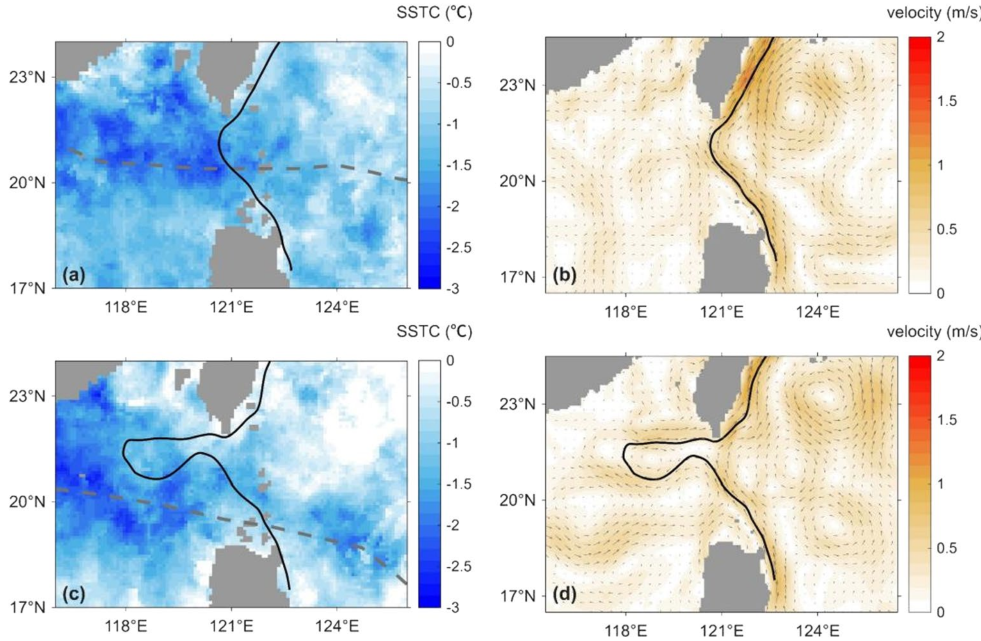

Fig. 1 Satellite-observed SSTC (shading, unit: °C) induced by TCs (**a**) Hato in 2017 and (**c**) Hagupit in 2008. Satellite-observed mean surface current fields (magnitude: shading; unit: m/s; direction: quivers) in (**b**) August 2017 and (**d**) September 2008. In each subfigure, the black solid curve denotes the major axis of the Kuroshio and the gray dashed curve represents the TC track

only focuses on the ocean's response to the TC, whereas the ocean's feedback on the TC is not considered.

The simulated domain is set to 115.5-126.5° E and 16.5–24.5° N, with a horizontal resolution of 1/20° (approximately 5 km). There are fifty uneven sigma layers in the vertical direction, with stretching parameters of 15.0 for THETA_S and 0.4 for THETA_B. A 50-km wide sponge layer with enhanced viscosity and diffusivity is set at the open boundaries to absorb baroclinic energy. The K-Profile Parameterization (KPP) vertical mixing scheme (Large et al. 1994) is implemented in the CROCO. The Laplacian background viscosity and diffusivity are set to 100 and 10 m^2/s, respectively. A linear bottom friction coefficient of 3.0×10^{-4} m/s is used. Bathymetric data are obtained from the 1 arc-minute global relief model (ETOPO1, Fig. 2a).

Four semi-idealized experiments are designed, of which the key settings are listed in Table 1. In Exps 1 and 2, the monthly averaged ocean conditions in November 2013 and November 2008 are used, when the Kuroshio took the looping and leaping paths, respectively (Fig. 2c and e). The initial and boundary conditions, including velocity, temperature, salinity and surface elevation, are derived from the monthly averaged Hybrid Coordinate Ocean Model (HYCOM) reanalysis data (https://www.hycom.org/). Exps 3 and 4 serve as the control experiments for Exps 1 and 2, respectively, in which the initial and boundary conditions are prescribed using the horizontally averaged temperature, salinity and surface elevation fields of the HYCOM reanalysis over the simulation domain. The velocity in both the initial state and at the open boundaries are set to zero in Exps 3 and 4. To focus on the influence of the Kuroshio, other factors such as tides and precipitation are not considered.

The same idealized TC is prescribed in the four experiments, traveling westward across the domain along 20.5°N (Figure 2b). Its parameters are determined based on the TC best-track data for the northern SCS (112–122°E, 16–24°N) from 2004 to 2015. According to the TC best-track data, the median (mean) values of the maximum wind speed, radius of maximum wind speed, and translation speed are 23.0 m/s (26.4 m/s), 46.0 km (44.6 km), and 3.30 m/s (3.79 m/s), respectively (Figure 3). Hence, the idealized TC is configured with a maximum wind speed of 30 m/s, a radius of maximum wind speed of 50 km, and a translation speed of 3 m/s, as a maximum wind speed of 20 m/s would be too low to represent a typical TC. The wind field of the TC is prescribed following Jelesnianski (1965):

$$W(r)=\begin{cases}\frac{r}{R+r}(V_x i+V_y j)+W_R\frac{1}{r}\left(\frac{r}{R}\right)^{\frac{3}{2}}(Ai+Bj),\ 0<r\le R\\ \frac{R}{R+r}(V_x i+V_y j)+W_R\frac{1}{r}\left(\frac{R}{r}\right)^{\frac{1}{2}}(Ai+Bj),\ r>R\end{cases} \quad (1)$$

where **W** is the wind speed vector, **i** and **j** are zonal and meridional unit vectors, r is the distance from the TC center, W_R is the maximum wind speed, R is the radius of the maximum wind speed, V_x and V_y are the zonal and meridional translation speeds of the TC, and

$$\begin{cases}A=-[(x-x_c)\sin\ \theta+(y-y_c)\cos\ \theta]\\ B=\ [(x-x_c)\cos\ \theta-(y-y_c)\sin\ \theta]\end{cases} \quad (2)$$

where (x, y) and (x_c, y_c) are the coordinates of grid and TC center, respectively, and θ is the ingress angle:

$$\theta=\begin{cases}20^\circ,\ r\le R\\ 15^\circ,\ r>R\end{cases} \quad (3)$$

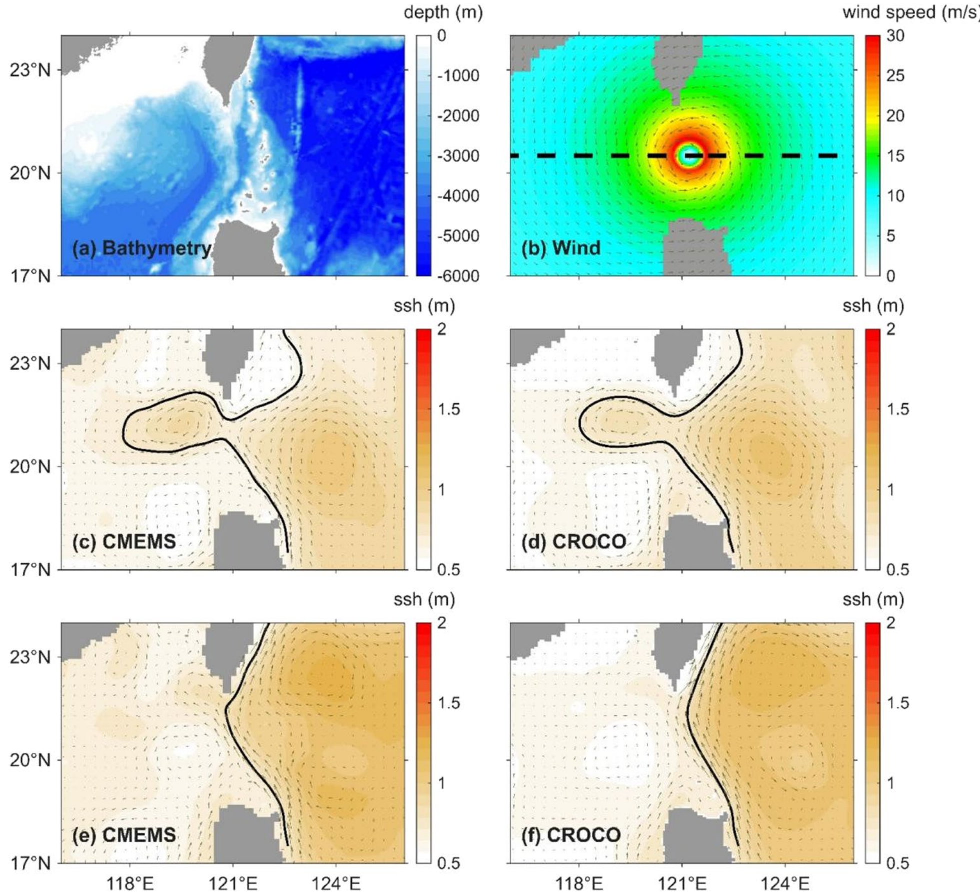

Fig. 2 (**a**) Bathymetry (shading, unit: m) in the simulated domain. (**b**) The wind field (magnitude: shading; unit: m/s; direction: quivers) when the TC passes over the LS. The black dashed line represents the TC track. Mean sea surface height (shading, unit: m) and mean surface current fields (quivers) in (**c** and **d**) november 2013 and (**e** and **f**) November 2008 for satellite observations (**c** and **e**) and (**d** and **f**) CROCO simulations. The black solid curve denotes the major axis of the Kuroshio

Table 1 Key settings of the four semi-idealized experiments

	Initial condition	Kuroshio status
Exp 1	Real ocean condition in November 2013	looping path
Exp 2	Real ocean condition in November 2008	leaping path
Exp 3	Horizontally averaged ocean condition in November 2013	no Kuroshio
Exp 4	Horizontally averaged ocean condition in November 2008	no Kuroshio

According to the wind field, the TC reaches the LS on the 5th day of the simulation (Fig. 2b). Moreover, since an idealized TC is adopted in these experiments, the surface heat flux is omitted, as it generally has little influence on TC-induced SSTC in most cases (e.g. Price 1981; Zhang et al. 2016; Cheng et al. 2024).

In each experiment, the CROCO is operated for 20 days with a baroclinic time step of 120 s, and the number of barotropic time steps between per baroclinic time step is set to 60. The simulated results are output every 1 h.

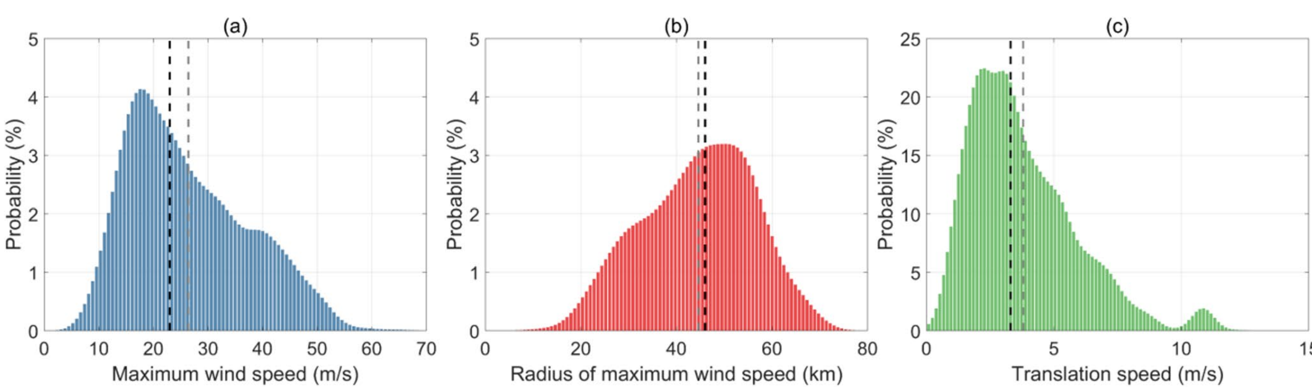

Fig. 3 Probabilities of the (**a**) maximum wind speed, (**b**) radius of maximum wind speed and (**c**) translation speed of all the TCs in the northern SCS from 2004 to 2015. The black and gray vertical dashed lines in each subfigure denote the median and mean values, respectively

2.2 Temperature equation in the mixed layer

According to the temperature equation in the mixed layer (Jullien et al., 2012), the variation of SST can be calculated as follows:

$$\frac{\partial SST}{\partial t} = \underbrace{-\frac{1}{h}\int_{-h}^{0}\left(u\frac{\partial T}{\partial x}+v\frac{\partial T}{\partial y}\right)dz}_{\text{Hadv}} \underbrace{-\frac{1}{h}\int_{-h}^{0} w\frac{\partial T}{\partial z}dz}_{\text{Vadv}} + \underbrace{\frac{1}{h}\int_{-h}^{0}K_l\left(\frac{\partial^2 T}{\partial x^2}+\frac{\partial^2 T}{\partial y^2}\right)dz}_{\text{Hmix}} + \underbrace{\left[-K_z\frac{1}{h}\frac{\partial T}{\partial z}(z=-h) - \frac{SST - T(z=-h)}{h}\frac{\partial h}{\partial t}\right]}_{\text{Vmix}} + \underbrace{\frac{Q}{\rho C_p h}}_{\text{Heat flux}} \quad (4)$$

where T is the temperature, t is the time, x and y are zonal and meridional coordinates, z is the depth, u, v and w are the zonal, meridional and vertical velocities, respectively, K_l and K_z are the horizontal and vertical mixing coefficients, respectively, and h is the time-varying MLD. The five terms on the right-hand side of Eq. (4) represent the horizontal advection (Hadv), vertical advection (Vadv), horizontal mixing (Hmix), vertical mixing (Vmix), and surface heat flux, respectively. In this study, the MLD is calculated as the depth at which the temperature is 0.5 °C lower than the temperature at 5 m depth (Sprintall and Tomczak 1992; Watanabe and Hibiya 2002; Cheng et al. 2023). In fact, using a density threshold criterion (0.125 kg m^{-3} larger than the surface value; Rimac et al. 2016) yields similar results (not shown). Because the surface heat flux is not considered in the four semi-idealized experiments, it is 0. The vertical mixing is generally considered to be the primary driver of the variation of SST (Price 1981; Greatbatch 1984; Shay et al. 1992; Jacob et al. 2000; Jullien et al. 2012; Qiao et al. 2022; Cheng et al. 2023, 2024), of which the first term is vertical diffusion at the MLD and the second term is entrainment (Vincent et al. 2012a; Jullien et al. 2012).

3 Result

3.1 Validation of the simulated Kuroshio

The CROCO-simulated Kuroshio patterns in November 2013 and November 2008 are illustrated in Fig. 2d and f. The simulated Kuroshio exhibits a looping path in November 2013 and a leaping path in November 2008, which is consistent with the satellite observations (Fig. 2c and e) downloaded from the Copernicus Marine Environment Monitoring Service (CMEMS, https://doi.org/10.48670/moi-00148), thereby demonstrating the reasonability and reliability of the simulated Kuroshio. The simulated sea surface heights averaged in the two periods (Fig. 2d and f) also match satellite observations (Fig. 2c and e), further confirming the credibility of the simulated results. Figure 4 compares the MLD distribution between the CROCO simulations and HYCOM reanalysis data three days before the TC's arrival. The CROCO-simulated MLD pattern is generally consistent with the HYCOM reanalysis data. When the Kuroshio exhibits a looping path, the MLD around the anticyclonic eddy induced by the looping Kuroshio is deeper. When the Kuroshio takes a leaping path, the MLD to the west side of the LS is shallower than that to the east side.

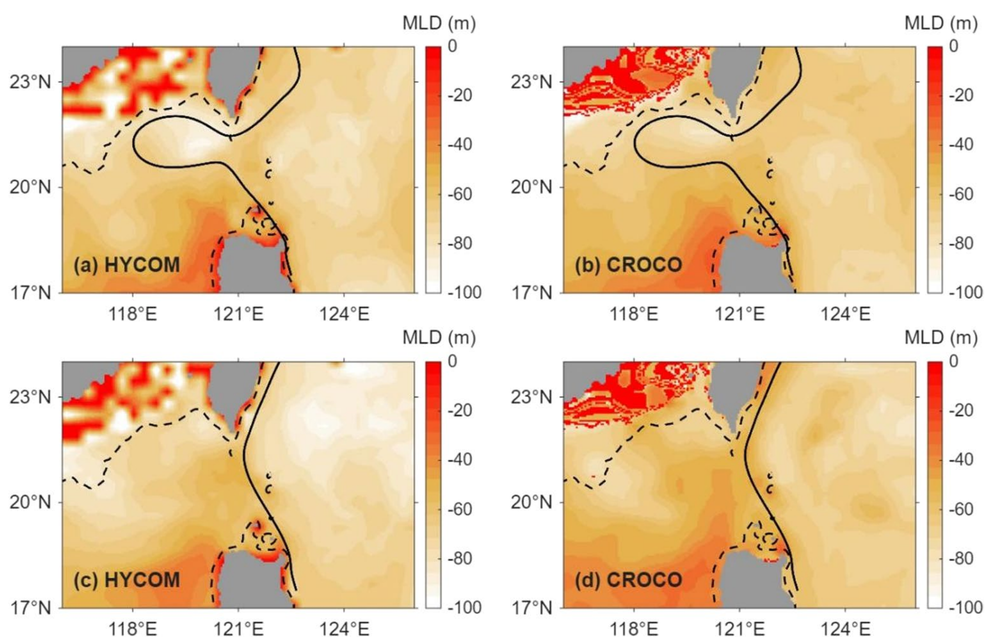

Fig. 4 MLD (shading, unit: m) in the simulated domain in (**a** and **b**) November 2013 and (**c** and **d**) November 2008 for (**a** and **c**) HYCOM reanalysis data and (**b** and **d**) CROCO simulations. In each subfigure, the black solid curve denotes the major axis of the Kuroshio and the black dashed curve denotes the 500 m isobath

3.2 TC-induced SSTC patterns

TC-induced SSTC is calculated as the difference between the minimum SST within 4 days after the TC's arrival and the SST 1 day before the TC's arrival. Figure 5 shows TC-induced SSTC in the four experiments as well as the difference of SSTC among different cases. Because this study mainly focuses on the Kuroshio's influence on TC-induced SSTC, which primarily occurs in deep waters, only results from waters deeper than 500 m are presented. Overall, the TC in the four experiments causes larger SSTC to the right side of TC track than to the left side, which is consistent with the rightward biased feature of ocean's response to a TC in the Northern Hemisphere (Price et al. 1994). Because horizontally homogeneous stratification is used and no background currents exist in Exps 3 and 4, the SSTC patterns in the two experiments are regular. In contrast, because the real ocean conditions including the non-homogeneous stratification and background currents are considered in Exps 1 and 2, the SSTC exhibits complicated patterns, showing evident differences to both sides of the LS. To further investigate the difference of SSTC in different experiments, two areas (the two boxes in Fig. 5) are selected: Area A (118.8-119.8 °E, 20.8–21.8 °N) is located in the anticyclonic eddy induced by the looping Kuroshio to the west side of the LS and Area B (121.0-122.0 °E, 20.8–21.8 °N) is located along the major axis of the leaping Kuroshio to the east side of the LS. Moreover, because both Exps 3 and 4 use the horizontally homogeneous stratification in November (although in different years), TC-induced SSTC in these two experiments is nearly the same, and the difference between them is too small to be noticed (Fig. 5e). Therefore, in the following analysis, only the results of Exp 3 is used to represent the no-Kuroshio case.

As shown in Fig. 5f, in comparison to the no-Kuroshio case (Exp 3), the looping Kuroshio (Exp 1) reduces TC-induced SSTC across nearly the entire region to the right of the TC track. In Exp 3, the SSTC in Areas A and B is −0.87 °C and −0.86 °C, respectively. In contrast, in the looping Kuroshio case (Exp 1), the SSTC in Areas A and B decreases to −0.71 °C and −0.73 °C, representing a reduction of 15–20%. In the leaping Kuroshio case (Exp 2), the SSTC within 120 km to the right side of the TC track in the Philippine Sea is suppressed, which is similar to the looping Kuroshio case. However, the leaping Kuroshio enhances the SSTC in the SCS Basin and the Kuroshio's downstream region (Fig. 5g). Consequently, under the influence of the leaping Kuroshio, the SSTC in Area A (Area B) is −0.99 °C (−0.55 °C) which is increased by 14% (decreased by 36%) compared to the no-Kuroshio case. These results confirm that the Kuroshio can affect the SSTC induced by the TC that passes over the LS.

When directly comparing TC-induced SSTC under the looping and leaping Kuroshio (Fig. 5h), it becomes evident that the looping and leaping Kuroshio exert different influences on the SSTC. Specifically, the looping Kuroshio notably reduces the SSTC in the anticyclonic eddy generated by the looping Kuroshio (Area A), while simultaneously causing an increase in the SSTC along the major axis of the leaping Kuroshio to the east side of the LS (Area B), compared to the leaping Kuroshio. These results further indicate that different Kuroshio intrusion types differently modulate the intensity and spatial pattern of TC-induced SSTC.

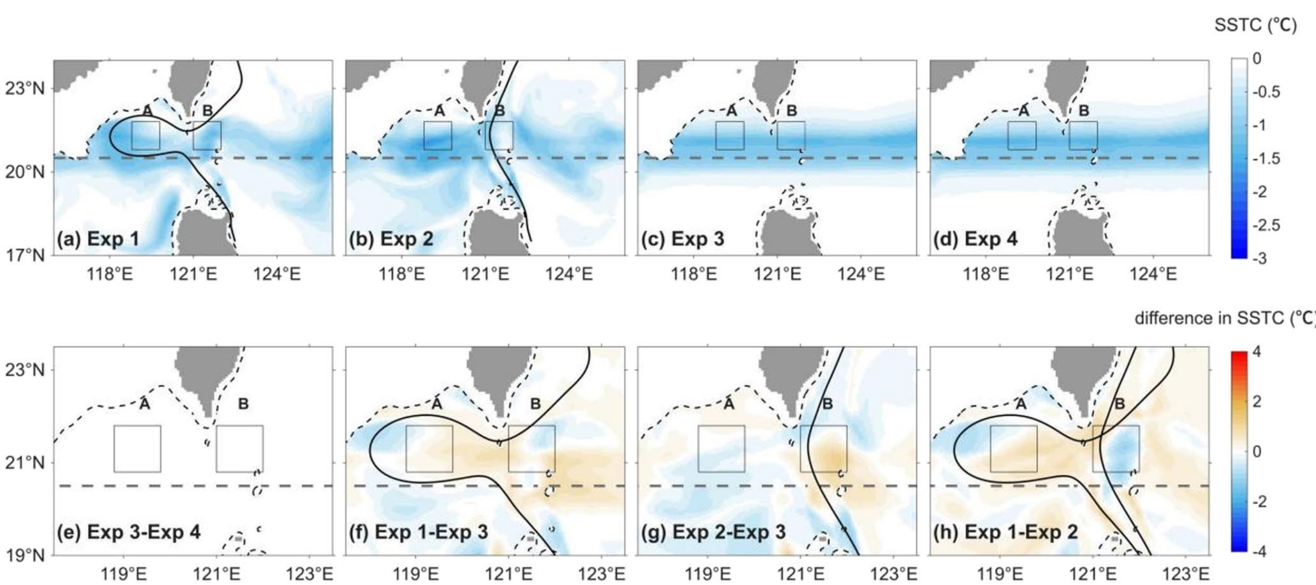

Fig. 5 TC-induced SSTC (shading, unit: °C) in (**a**) Exp 1, (**b**) Exp 2, (**c**) Exp 3 and (**d**) Exp 4. Difference of SSTC between (**e**) Exps 3 and 4, (**f**) Exps 1 and 3, (**g**) Exps 2 and 3 and (**h**) Exps 1 and 2. In each subfigure, the gray dashed line denotes the TC track, the black solid curve represents the major axis of the Kuroshio, the black dashed curve is the 500 m isobath and the two boxes denote the selected research areas

3.3 Analysis of temperature equation in the mixed layer

To further understand why different Kuroshio paths have different influences on TC-induced SSTC, analysis of temperature equation in the mixed layer (Eq. 4) is performed. Figure 6 shows the derivative of SST with respect to time (the left-hand side of Eq. 4), the contributions of vertical mixing, horizontal mixing, vertical advection and horizontal advection to the derivative of SST (the right-hand side of Eq. 4), as well as the temporal variation of MLD. Time zero (0 h) represents the moment when the TC center reaches the center of Area A or B. Due to the horizontally homogeneous initial stratification employed in Exp 3, the results in Areas A and B exhibit minimal differences, eliminating the need for separate analysis of them. In all the three experiments, the contributions of horizontal mixing are nearly zero (Fig. 6c), which can be neglected. The vertical advection can enhance SSTC by transporting cold water from the deeper ocean to the surface (Price 1981; Chiang et al. 2011). Because of the same TC and similar stratification in November, the contributions of vertical advection are nearly the same in the two Areas and in all the experiments (Fig. 6d). Hence, neither horizontal mixing nor vertical advection is the primary cause for the different SSTC introduced above (Fig. 5). The vertical mixing (Fig. 6b) exhibits a similar varying trend as the derivative of SST (Fig. 6a), indicating that the SSTC is primarily controlled by the vertical mixing, which is consistent with previous studies (Price 1981; Greatbatch 1984; Shay et al. 1992; Jacob et al. 2000; Jullien et al. 2012; Qiao et al. 2022; Cheng et al. 2023, 2024). Moreover, the horizontal advection varies in different Areas and in different experiments (Fig. 6e), suggesting that it is also crucial in the TC-induced SSTC under the influence of different Kuroshio intrusion types. Therefore, we will mainly focus on vertical mixing and horizontal advection in the following analysis.

3.4 Vertical mixing

As introduced above, vertical mixing dominates TC-induced SSTC, which manifests distinct characteristics in different Areas for different Kuroshio intrusion types (Fig. 6b). To delve deeper into the variations of vertical mixing in different scenarios, Fig. 7 shows the spatial patterns of vertical mixing in the simulated domain and Fig. 8 illustrates the factors that govern vertical mixing in the three experiments.

As shown in Fig. 7a-c, vertical mixing exhibits different spatial patterns for different Kuroshio intrusion types. In the no-Kuroshio case (Exp 3), enhanced vertical mixing mainly appears to the right side of the TC track in both the SCS and Philippine Sea (Fig. 7c), which is consistent with TC-induced SSTC pattern (Fig. 5c). In the looping Kuroshio case (Exp 1), enhanced vertical mixing mainly occurs along the looping Kuroshio path to the south of 21°N in the SCS and in Area B to the east of the LS, and the vertical mixing in the Philippine Sea is relatively weak (Fig. 7a). However, in the leaping Kuroshio case (Exp 2), enhanced vertical mixing is found to appear from the major axis of the Kuroshio at

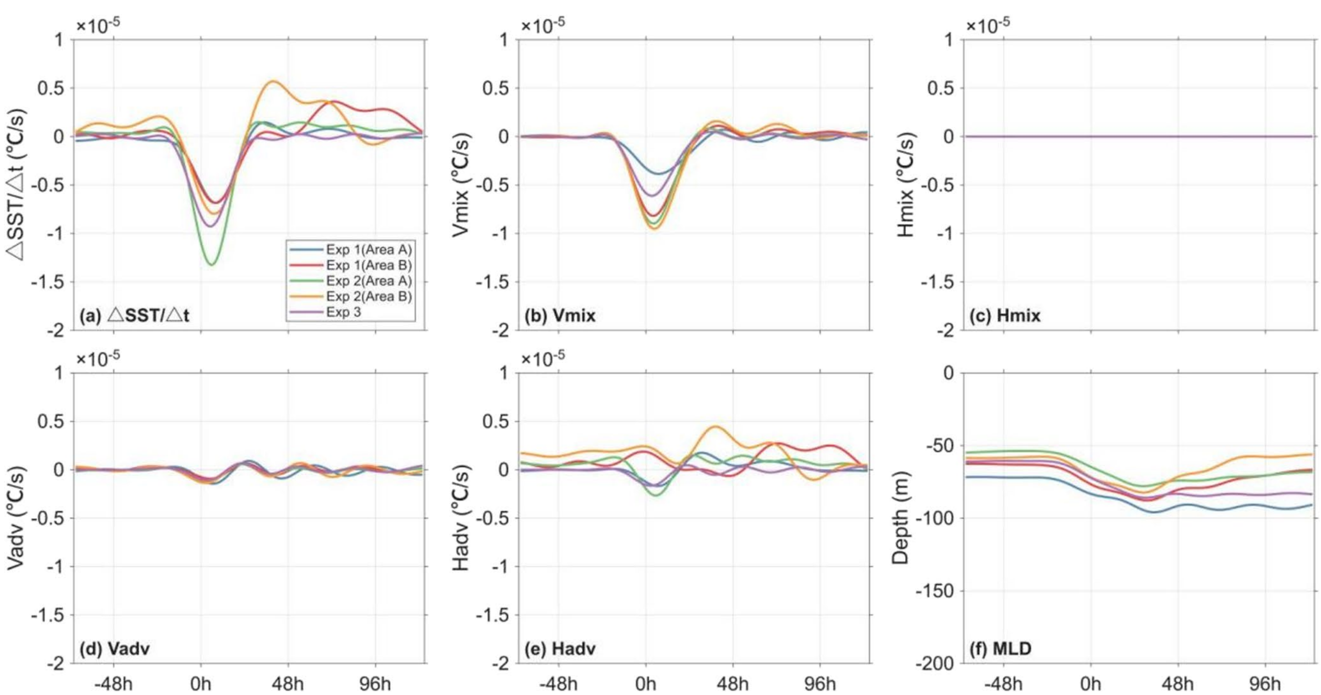

Fig. 6 (**a**) Derivative of SST with respect to time and contributions of (**b**) vertical mixing, (**c**) horizontal mixing, (**d**) vertical advection and (**e**) horizontal advection to derivative of SST, as well as (**f**) temporal variation of MLD in areas A and B in Exps 1-3

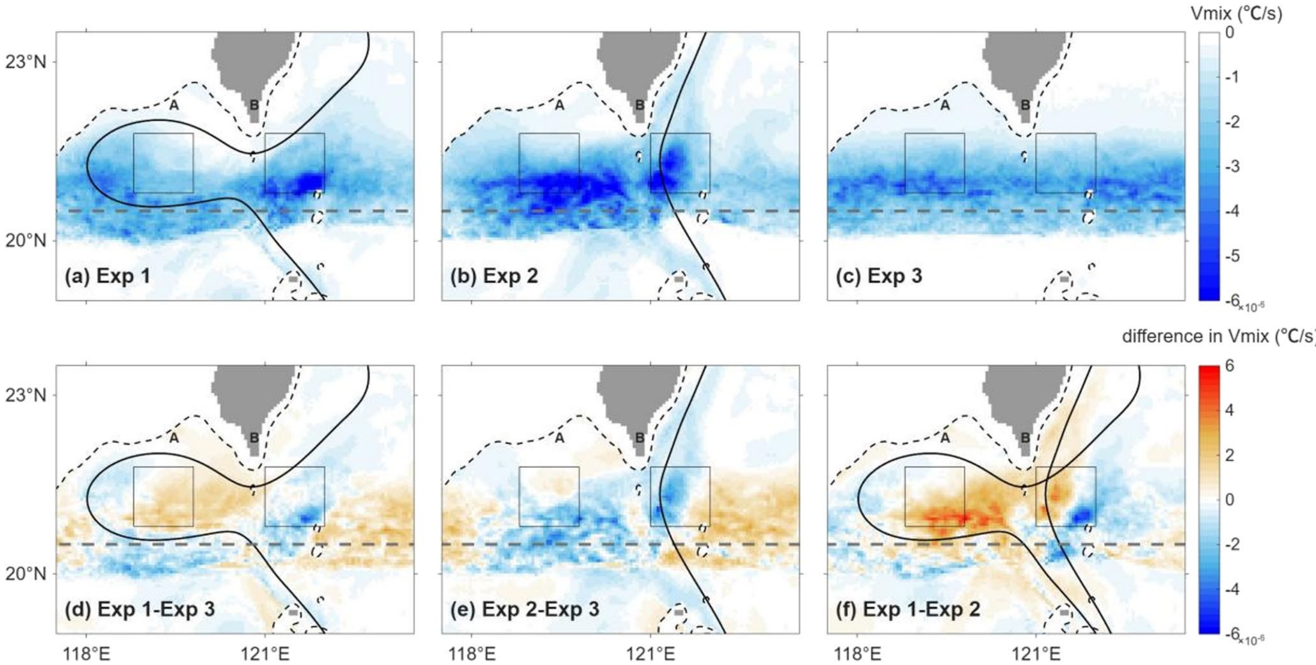

Fig. 7 Vertical mixing averaged from −24 to 48 h (shading, unit: °C/s) in (**a**) Exp 1, (**b**) Exp 2 and (**c**) Exp 3. Difference of time-averaged vertical mixing between (**d**) Exps 1 and 3, (**e**) Exps 2 and 3 and (**f**) Exps 1 and 2. In each subfigure, the gray dashed line denotes the TC track, the black solid curve represents the major axis of the Kuroshio, the black dashed curve is the 500 m isobath and the two boxes denote the selected research areas

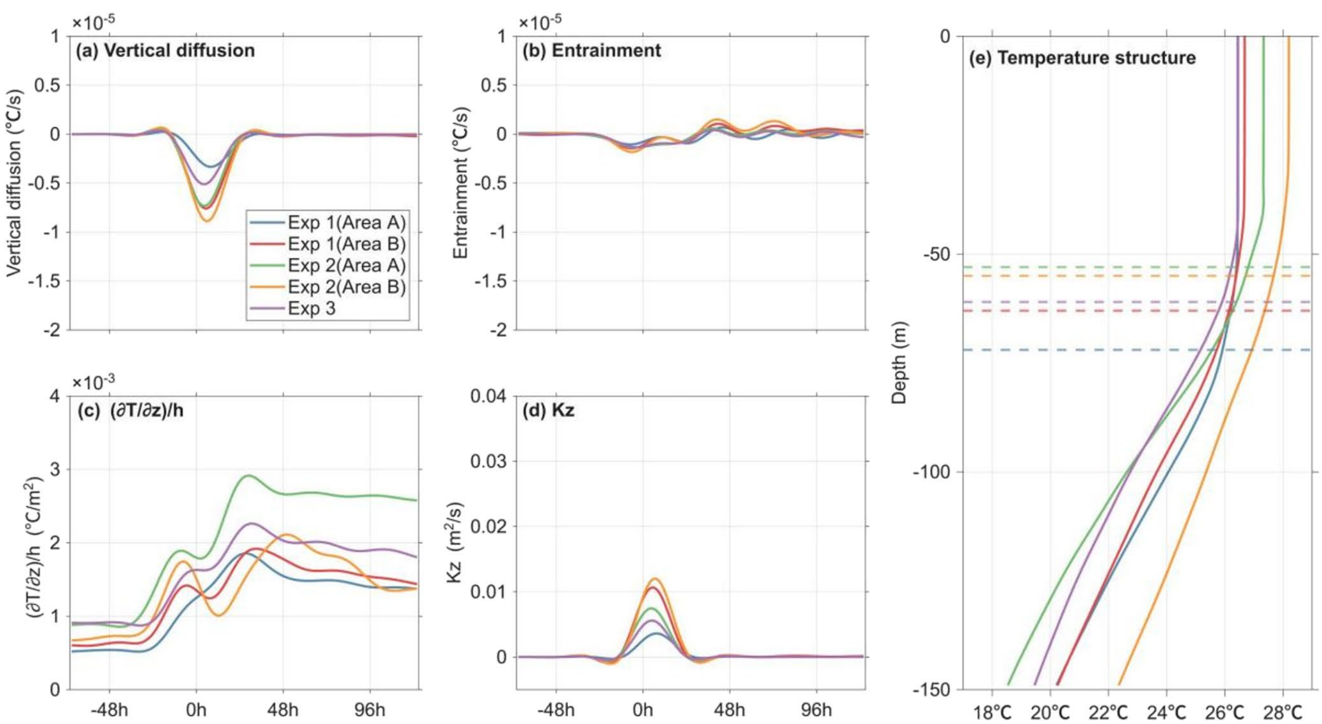

Fig. 8 (**a**) Vertical diffusion at the MLD, (**b**) entrainment, (**c**) temperature gradient divided by the MLD, (**d**) vertical mixing coefficient at the MLD and (**e**) vertical temperature structure 1 day before TC's arrival in Areas A and B in Exps 1-3. The dashed lines in subfigure (**e**) represent the corresponding MLDs

the LS to 118°E in the SCS, while the vertical mixing in the Philippine Sea also keeps a relatively low level (Fig. 7b). As a result, the looping Kuroshio suppresses the vertical mixing in Area A but enhances it in Area B (Fig. 7d), whereas the leaping Kuroshio enhances the vertical mixing in both Areas A and B (Fig. 7e), compared to the no-Kuroshio case. A direct comparison of vertical mixing under the looping and leaping Kuroshio (Fig. 7f) reveals that the anticyclonic eddy generated by the looping Kuroshio suppresses vertical mixing in Area A. In Area B, the looping Kuroshio weakens vertical mixing in the left half but enhances it in the right half, possibly due to its northward branch to the east side of the LS (Fig. 5d).

The vertical mixing is dominated by the vertical diffusion (Fig. 8a) over entrainment (Fig. 8b) in all these cases, which is consistent with previous studies (Cheng et al. 2023; 2024). Hence, the different intensities of vertical mixing can be explained by the temperature gradient divided by the MLD [$(\partial T/\partial z)/h$] and vertical mixing coefficient at the MLD (K_z) shown in Fig. 8c and d.

In the looping Kuroshio case (Exp 1), the values of $(\partial T/\partial z)/h$ in both Areas A and B are smaller than that in the no-Kuroshio case (Exp 3), which is due to the warmer subsurface water, smaller vertical temperature gradient and larger MLD (Fig. 8e). At the same time, the vertical mixing coefficient K_z in Area B is larger in the looping Kuroshio case than in the no-Kuroshio case, whereas the K_z in Area A is smaller in the looping Kuroshio case than in the no-Kuroshio case (Fig. 8d). This difference is because the deeper MLD in the anticyclonic eddy generated by the looping Kuroshio weakens TC-induced near-inertial oscillations in the mixed layer and reduces the intensity of vertical mixing (Shay et al. 2000; Jaimes and Shay 2010; He et al. 2022). All these factors finally yield stronger vertical mixing in Area B and weaker vertical mixing in Area A under the influence of the looping Kuroshio (Fig. 6b).

In the leaping Kuroshio case (Exp 2), vertical mixing in both Areas is stronger than that in the no-Kuroshio case (Fig. 6b), but for different reasons. In Area A, because the leaping Kuroshio does not intrude into the SCS, the subsurface temperature gradient is larger and the MLD is smaller (Fig. 8e), resulting in a larger value of $(\partial T/\partial z)/h$ (Fig. 8c). This is the major cause for the enhanced vertical mixing in Area A. In Area B, by contrast, the enhanced vertical mixing is mainly attributed to the larger Kz induced by strong background currents of the leaping Kuroshio (Fig. 8d).

3.5 Horizontal advection

While vertical mixing dominates SSTC (Fig. 6), the variations in SSTC cannot be fully accounted for by the differences of vertical mixing across the experiments. For example, compared to the no-Kuroshio case (Exp 3), the vertical mixing in Area B is enhanced under both the looping and leaping Kuroshio (Fig. 6b), but the SSTC is reduced in both cases (Fig. 5f and g). This is because horizontal advection also plays a crucial role in TC-induced SSTC, due to the strong Kuroshio currents (Wu et al. 2008; He et al. 2022). To have a better understanding of horizontal advection, Fig. 9 illustrates the spatial distribution of horizontal advection averaged from −24 to 48 h, the period during which SSTC mainly occurs, in Exps 1–3.

In the no-Kuroshio case (Exp 3), the horizontal advection pattern is regular, which is positive below the TC track and negative to the right side of the TC track (Fig. 9c), suggesting that the horizontal advection transports cold water to the right side of the TC track (Zhang et al. 2016), contributing to the TC-induced SSTC. However, horizontal advection exhibits more complicated patterns under the influences of different Kuroshio intrusion types (Fig. 9a and b). In Area A, the spatial patterns of horizontal advection under both the leaping and looping Kuroshio are generally similar to that in the no-Kuroshio case, which is positive below the TC track and negative to the right side of the TC track. The different influences of the leaping and looping Kuroshio embody in the intensity and range of horizontal advection. However, in Area B to the east side of the LS, the horizontal advection is mainly positive under both the leaping and looping Kuroshio, which is different from that in the no-Kuroshio case, indicating that horizontal advection suppresses TC-induced SSTC here. This suppression explains why the SSTC is weaker in Area B for Exps 1 and 2 compared to Exp 3.

The differences of horizontal advection between the looping (leaping) Kuroshio and no-Kuroshio cases are clearly illustrated in Fig. 9d and e. As for the different influence between the looping and leaping Kuroshio, it is found that the positive and negative horizontal advection differences are generally eliminated in Area A; but in Area B, the leaping Kuroshio causes stronger horizontal advection than the looping Kuroshio (Fig. 9f). Given that the vertical mixing in Area B is nearly comparable under the looping and leaping Kuroshio (Fig. 6b), this result explains why the SSTC in Area B is greater in Exp 1 (−0.73 °C) than in Exp 2 (−0.55 °C).

It should be noted that in addition to suppressing TC-induced SSTC, the horizontal advection also contributes to the temperature recovery (Fig. 6a). For example, after 48 h, the positive horizontal advection in Area B in the leaping Kuroshio case (Exp 2) causes faster temperature recovery (positive value of $\Delta SST/\Delta t$) than that in the no-Kuroshio case (Exp 3). Similar phenomenon is also found in Area B in the looping Kuroshio case (Exp 1). However, in Area A, such phenomenon is absent.

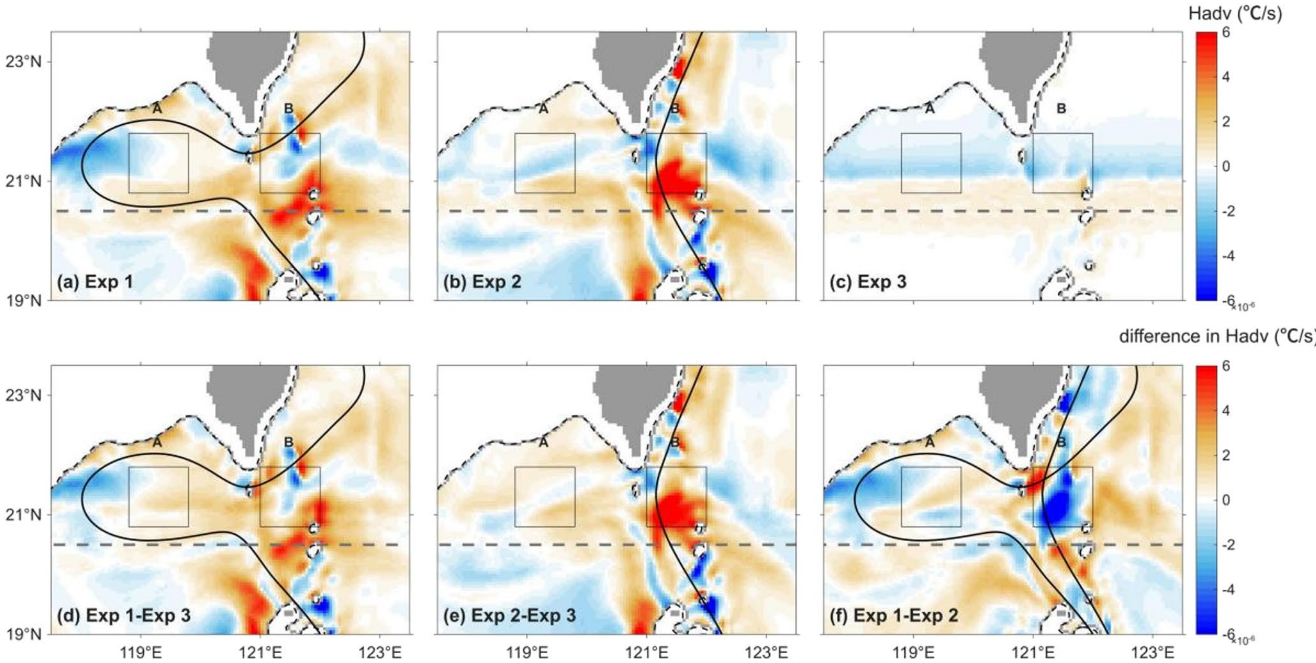

Fig. 9 Horizontal advection averaged from −24 to 48 h (shading, unit: °C/s) in (**a**) Exp 1, (**b**) Exp 2 and (**c**) Exp 3. Difference of time-averaged horizontal advection between (**d**) Exps 1 and 3, (**e**) Exps 2 and 3 and (**f**) Exps 1 and 2. In each subfigure, the gray dashed line denotes the TC track, the black solid curve represents the major axis of the Kuroshio, the black dashed curve is the 500 m isobath and the two boxes denote the selected research areas

4 Discussions

Through numerical simulations, this study explores the influence of the Kuroshio intrusion into the SCS on TC-induced SSTC. It is found that TC-induced SSTC is weakened by the Kuroshio and the recovery of SST is faster to the east side of the LS, which is due to the temperature horizontal advection by the Kuroshio. These findings are consistent with previous studies (Wu et al. 2008; Liu and Wei 2015; He et al. 2022). Moreover, because the leaping Kuroshio is faster and less dispersed than the looping Kuroshio, the former causes stronger horizontal advection to the east side of the LS than the latter (Fig. 9f).

He et al. (2022) proposed that the Kuroshio had a thicker mixed layer and removed the wind energy transferred to the mixed layer, thereby suppressing TC-induced SSTC. Our simulated results in Area A under the influence of the looping Kuroshio exhibit similar characteristics (Figs. 5f and 6d and e) to this mechanism. However, in Area B under the influence of the leaping Kuroshio, vertical mixing is enhanced rather than suppressed (Fig. 6b), and the MLD is even shallower than that in the no-Kuroshio case (Fig. 8e). This indicates that the observed suppression of SSTC in Area B under the influence of the leaping Kuroshio (Fig. 5g) cannot be attributed to the mechanism described by He et al. (2022). In fact, the enhanced vertical mixing in Area B under the influence of the leaping Kuroshio is more consistent with the finding of Wei et al. (2014), who demonstrated that enhanced vertical mixing is attributed to kinetic energy extraction from the Kuroshio's baroclinic potential energy. However, in Area B, the SSTC is still suppressed by the leaping Kuroshio (Fig. 5g). This is because the horizontal advection of the leaping Kuroshio eliminates TC-induced SSTC to some extent (Fig. 9e). This highlights the role of horizontal advection in modulating TC-induced SSTC, although it is usually negligible due to its substantially smaller contribution than the vertical mixing and vertical advection in most other scenarios (e.g. Zhang 2023; Cheng et al. 2023; 2024).

Although the Kuroshio paths vary seasonally (Nan et al. 2011, 2015), their modulation on TC-induced SSTC is not month-dependent. This is supported by Fig. 10, which shows the results for the leaping Kuroshio in August 2011 (Fig. 10a) and the looping Kuroshio in December 2007 (Fig. 10d), using the same idealized TC as in Exps 1–4. Relative to their respective control experiments (Fig. 10b and e), the leaping Kuroshio enhances SSTC to the east side of the LS but suppresses it to the west (Fig. 10c), whereas the looping Kuroshio weakens SSTC to both sides of the LS (Fig. 10f). These results are consistent with those obtained from Exps 1–4, demonstrating the robustness of our findings regarding the Kuroshio's influence on TC-induced SSTC.

Furthermore, the influence mechanism of the Kuroshio on TC-induced SSTC is also independent on TC characteristics. Figure 11 shows the SSTC induced by TCs with

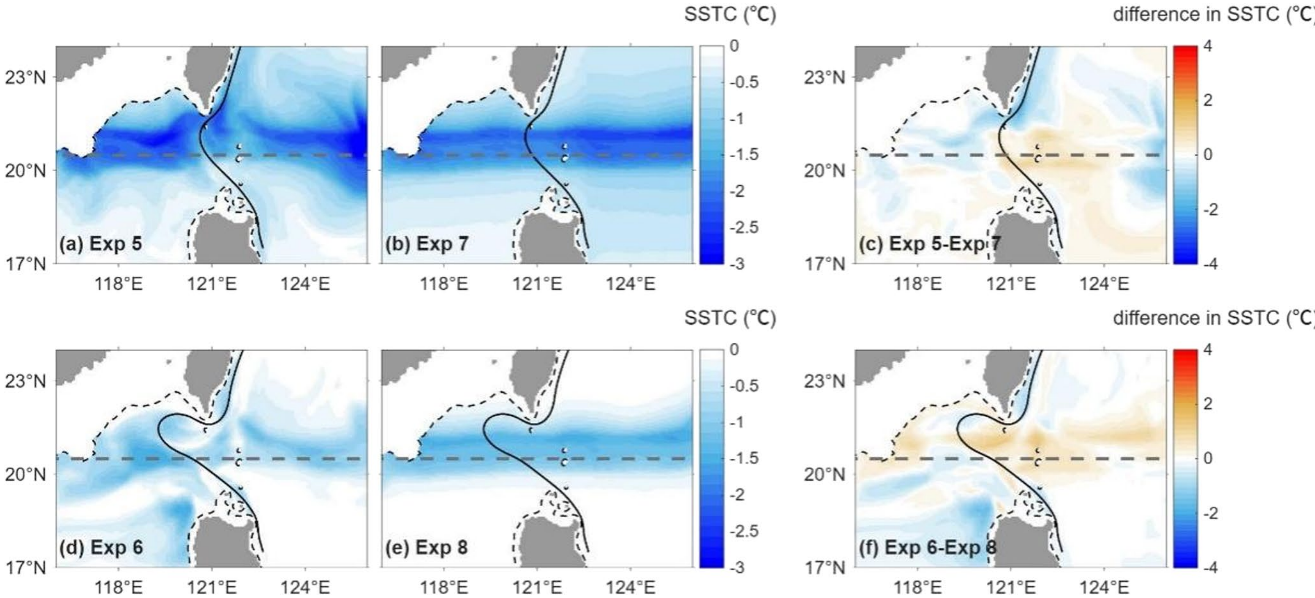

Fig. 10 TC-induced SSTC (shading, unit: °C) in (**a**) Exp 5 (leaping Kuroshio in August 2011), (**d**) Exp 6 (looping Kuroshio in December 2007), (**b**) Exp 7 (no Kuroshio in August 2011) and (**e**) Exp 8 (no Kuroshio in August 2007). Difference of SSTC between (**c**) Exps 5 and 7 and (**f**) Exps 6 and 8. In each subfigure, the gray dashed line denotes the TC track, the black solid curve represents the major axis of the Kuroshio, the black dashed curve is the 500 m isobath

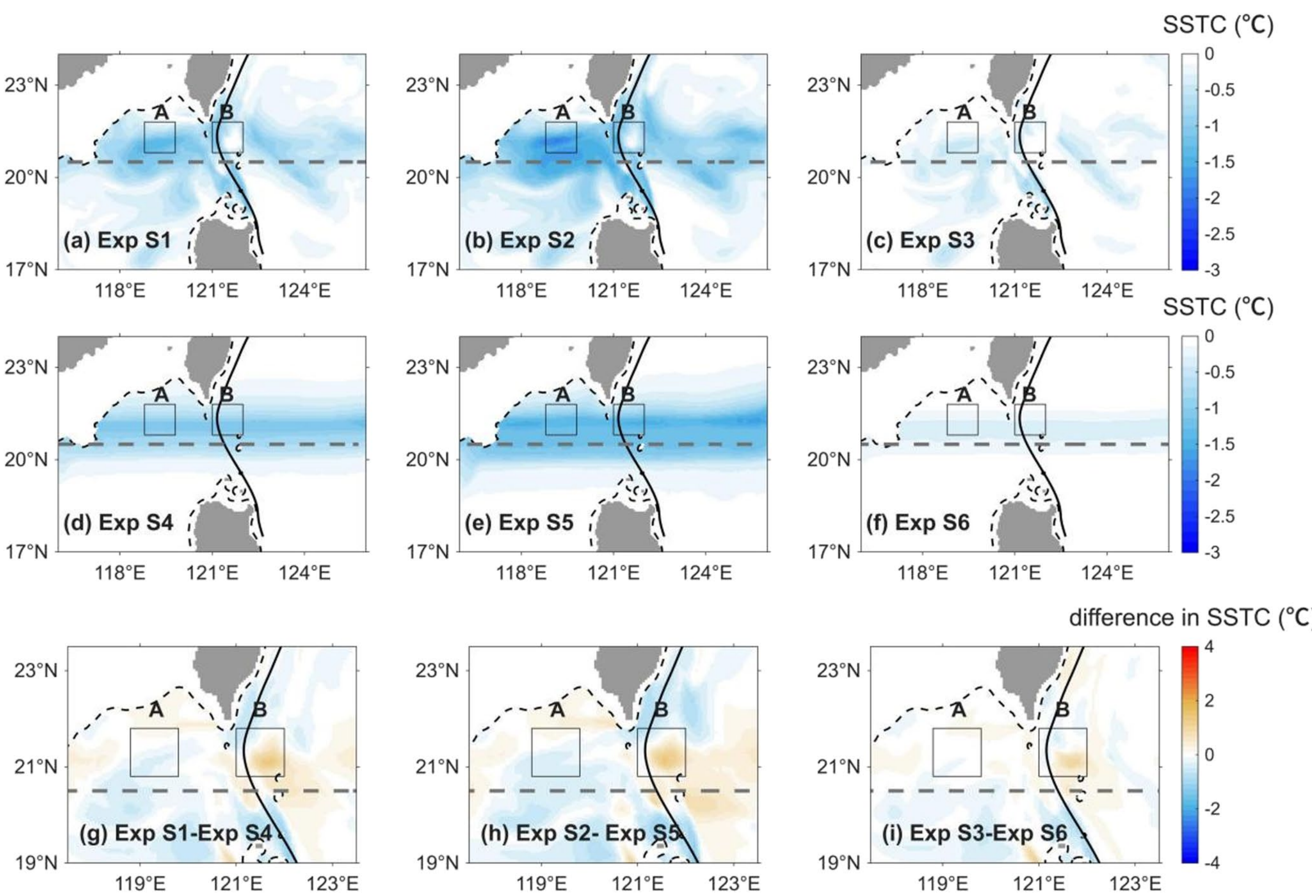

Fig. 11 TC-induced SSTC (shading, unit: °C) in (**a**) Exp S1, (**b**) Exp S2, (**c**) Exp S3, (**d**) Exp S4, (**e**) Exp S5 and (**f**) Exp S6. Difference of SSTC between (**g**) Exps S1 and S4, (**h**) Exps S2 and S5, (**i**) Exps S3 and S6. In each subfigure, the gray dashed line denotes the TC track, the black solid curve represents the major axis of the Kuroshio, the black dashed curve is the 500 m isobath and the two boxes denote the selected research areas

different characteristics (sensitivity experiments S1-S3), under the same leaping Kuroshio condition as in Exp 2. In these sensitivity experiments, only one TC parameter, either the maximum wind speed, the radius of maximum wind speed, or the translation speed, is changed, while all other settings are kept invariant. Specifically, in Exp S1, the translation speed is set to 4 m/s; in Exp S2, the radius of maximum wind speed is set to 60 km; and in Exp S3, the maximum wind speed is set to 20 m/s. Exps S4-S6 serve as the control experiments for Exps S1-S3, respectively, with only the ocean condition replaced by that of Exp 4. As shown, the SSTC varies consistently with changes in TC characteristics (Figs. 11a-f), which aligns with previous studies (e.g., Lin et al. 2008; 2009; Cheng et al. 2023; Liu et al. 2023). However, the SSTC difference for each pair of control experiments (Figs. 11g-i) exhibits a highly similar pattern: the SSTC is enhanced to the west side of the LS but weakened to the east side.

Exps R1-R6 are identical to Exps S1-S6, except that they are conducted under the looping Kuroshio path. As shown in Fig. 12, the SSTC difference for each pair of control experiments is similar to that between Exp1 and Exp3, with SSTC being suppressed in both Areas A and B. The temperature equation analysis for these experiments (not shown) also yields results consistent with those presented in Sect. 3, further confirming that the Kuroshio's influence on TC-induced SSTC is robust and independent of TC characteristics.

Previous studies also indicated that when a TC traverses the major axis of the Kuroshio, TC-induced SSTC spreads downstream along the major axis of the Kuroshio, owing to the Kuroshio's transport of TC-induced cold water (Liu and Wei 2015; He et al. 2022). Such phenomenon is reproduced in the leaping Kuroshio case (Fig. 5b). However, our results suggest that the SSTC in the downstream region of the leaping Kuroshio is driven by vertical mixing rather than horizontal advection. Compared to the no-Kuroshio case, the downstream region exhibits a negative vertical mixing difference (Fig. 7e) but a positive horizontal advection difference (Fig. 9e). The former tends to enhances SSTC, while the latter tends to suppresses it.

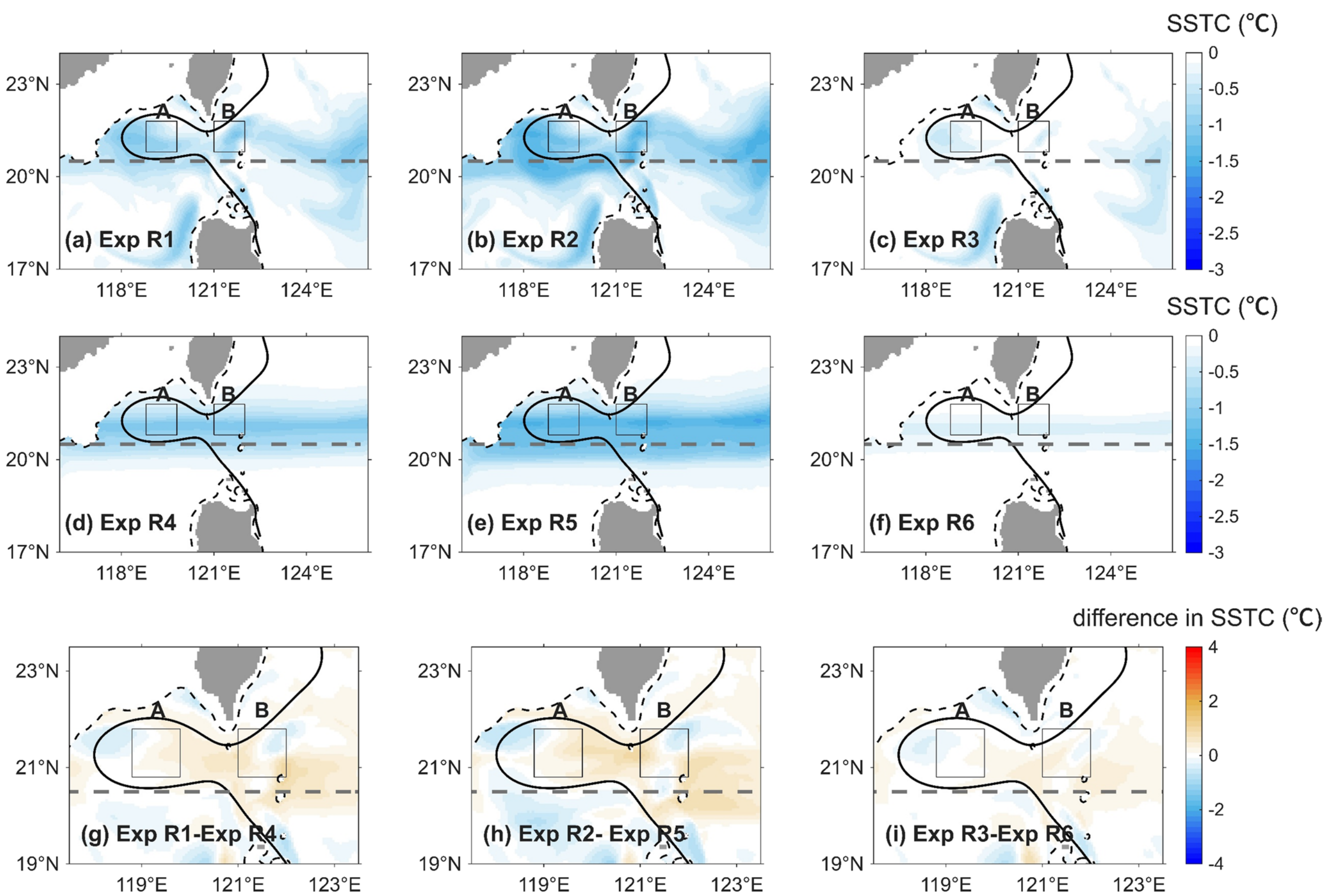

Fig. 12 TC-induced SSTC (shading, unit: °C) in (**a**) Exp R1, (**b**) Exp R2, (**c**) Exp R3, (**d**) Exp R4, (**e**) Exp R5 and (**f**) Exp R6. Difference of SSTC between (**g**) Exps R1 and R4, (**h**) Exps R2 and R5, (**i**) Exps R3 and R6. In each subfigure, the gray dashed line denotes the TC track, the black solid curve represents the major axis of the Kuroshio, the black dashed curve is the 500 m isobath and the two boxes denote the selected research areas

Despite the findings presented above, this study has several limitations. First, TC-induced surface waves are intense and play an important role in modifying MLD and upper ocean mixing (e.g. Zhang et al. 2023a, b; Jing et al. 2025a, b), thereby affecting TC-induced SSTC. However, due to the present model configurations, the influence of TC-induced surface waves is not considered. Second, the influence of internal tides generated at the LS on TC-induced SSTC is also excluded. Previous studies have demonstrated that internal tides can modulate TC-induced SSTC near the LS (Cheng et al. 2023; Guan et al. 2024), but internal tides are also influenced by different Kuroshio paths (Jan et al. 2012; Kerry et al. 2014a, b; Xu et al. 2021; Cao et al. 2022, 2026). Incorporating internal tides into the model would therefore complicate the research question addressed here. To isolate the direct influence of different Kuroshio paths on TC-induced SSTC, tidal forcing is omitted from the model configurations in the present study. These two issues will be explored in the future.

5 Summary

This study investigates the modulation of the Kuroshio intrusion into the SCS on TC-induced SSTC near the LS. The looping and leaping paths (Nan et al. 2011, 2015) of the Kuroshio are considered with the no-Kuroshio case as a comparison. In order to control variables, the same idealized TC prescribed by Jelesnianski (1965) is used. Due to the complexity of TC-ocean negative feedback mechanism, this study specifically examines the ocean's response to the TC.

Results demonstrate that both the looping and leaping Kuroshio modify TC-induced SSTC compared to the no-Kuroshio scenario, with distinct mechanisms. For the looping Kuroshio, the warmer subsurface water, smaller vertical temperature gradient and larger MLD account for the weaker vertical mixing in the anticyclonic eddy induced by the looping Kuroshio to the west side of the LS, which finally results in suppressed SSTC. To the east side of the LS, the SSTC is also suppressed, which is due to horizontal advection. For the leaping Kuroshio, reduced SSTC also occurs to the east side of the LS due to horizontal advection. Because the leaping Kuroshio is more tightly confined to the east side of the LS, it generates stronger horizontal advection than the looping Kuroshio, resulting in more pronounced suppression of TC-induced SSTC in this region. However, in the SCS Basin to the west side of the LS, the leaping Kuroshio enhances TC-induced SSTC, which is related to the enhanced vertical mixing. Moreover, it is found that TC-induced SSTC spreads downstream along the major axis of the leaping Kuroshio. Analysis indicates that this phenomenon is caused by vertical mixing rather than by horizontal advection.

Acknowledgements We acknowledge the supporting of projects listed in the Funding section.

Author contributions Shukui Cheng: Methodology; Formal analysis; Visualization; Writing—original draft; Writing—review & editing. Anzhou Cao: Conceptualization; Writing—original draft; Writing—review & editing. Jinbao Song: Supervision; Writing—review & editing. Xinyu Guo: Supervision; Writing—review & editing.

Funding This study is partly supported by the Zhejiang Provincial Natural Science Foundation of China (Grant Number: LZ25D060002), the Fundamental Research Funds for the Central Universities (Grant Number: 226-2025-00150), and the Ministry of Education, Culture, Sports, Science and Technology, Japan (MEXT) to a project on Joint Usage/Research Center-Leading Academia in Marine and Environment Pollution Research (LaMer). Anzhou Cao acknowledges the Funding of ZJU Tang Scholar.

Data availability The CROCO code is available at https://www.croco-ocean.org. The ETOPO1 bathymetry data are available at https://www.ngdc.noaa.gov/mgg/global/relief/ETOPO1/tiled/. The geostrophic sea water velocity data are available at https://doi.org/10.48670/moi-00148. The TC best track data are available at http://tcdata.typhoon.org.cn. The HYCOM reanalysis data are available at https://www.hycom.org/. The remote sensing sea surface temperature data are available at https://www.remss.com/measurements/sea-surface-temperature/.

Declarations

Competing interests The authors declare no competing interests.

References

Cao A, Guo Z, Wang S, Guo X, Song J (2022) Incoherence of the M2 and K1 internal tides radiated from the Luzon Strait under the influence of looping and leaping Kuroshio. Prog Oceanogr 206:102850. https://doi.org/10.1016/j.pocean.2022.102850

Cao A, Guo Z, Chen X, Guo X, Song J (2026) Modulation of the Kuroshio current on the M2 internal tide energetics at the Luzon Strait. J Phys Oceanogr 56:1159–1172. https://doi.org/10.1175/JPO-D-25-0083.1

Chen H, Qiao F, Ezer T, Yuan Y, Hua F (2009) Multi-core structure of the Kuroshio in the East China Sea from long-term transect observations. Ocean Dynam 59(3):477–488. https://doi.org/10.1007/s10236-009-0182-9

Cheng S, Cao A, He H, Li P, Song J (2023) Numerical study on the influence of internal tides on tropical-cyclone-induced sea surface temperature cooling in the South China Sea. Ocean Dynam 73(7):449–461. https://doi.org/10.1007/s10236-023-01561-z

Cheng S, Cao A, Song J, Guo X (2024) Contribution of high-mode near-inertial waves to enhanced typhoon-induced sea surface temperature cooling in the South China Sea. Ocean Model 192:102452. https://doi.org/10.1016/j.ocemod.2024.102452

Chiang T, Wu C, Oey L (2011) Typhoon Kai-Tak: An Ocean's Perfect Storm. J Phys Oceanogr 41(1):221–233. https://doi.org/10.1175/2010JPO4518.1

Chou W, Gong G, Hung C, Wu Y (2013) Carbonate mineral saturation states in the East China Sea: present conditions and future scenarios. Biogeosciences 10. https://doi.org/10.5194/bg-10-6453-2013

Cui H, Tang D, Mei W, Liu H, Sui Y, Gu X (2023) Predicting tropical cyclone-induced sea surface temperature responses using machine learning. Geophys Res Lett 50(18):e2023GL104171. https://doi.org/10.1029/2023GL104171

D'Asaro E, Black P, Centurioni L, Harr P, Jayne S, Lin I et al (2011) Typhoon-ocean interaction in the Western North Pacific: part 1. Oceanography 24:24–31. https://doi.org/10.5670/oceanog.2011.91

Dare RA, McBride JL (2011) The threshold sea surface temperature condition for tropical cyclogenesis. J Clim 24(17):4570–4576. https://doi.org/10.1175/JCLI-D-10-05006.1

Deser C, Alexander MA, Timlin MS (1996) Upper-ocean thermal variations in the North Pacific during 1970–1991. J Clim 9(8):1840–1855. https://doi.org/10.1175/1520-0442(1996)009<1840:UOTVIT>2.0.CO;2

Emanuel K, DesAutels C, Holloway C, Korty R (2004) Environmental control of tropical cyclone intensity. J Atmos Sci 61(7):843–858. https://doi.org/10.1175/1520-0469(2004)061<0843:ECOTCI>2.0.CO;

Greatbatch RJ (1984) On the response of the ocean to a moving storm: parameters and scales. J Phys Oceanogr 14(1):59–78. https://doi.org/10.1175/1520-0485(1984)014<0059:OTROTO>2.0.CO;2

Guan S, Jin F, Tian J, Lin I, Pun I, Zhao W et al (2024) Ocean internal tides suppress tropical cyclones in the South China Sea. Nat Commun 15(1):3903. https://doi.org/10.1038/s41467-024-48003-y

He S, Cheng X, Fei J, Wei Z, Huang X, Liu L (2022) Thermal response to tropical cyclones over the Kuroshio. Earth Space Sci 9(5):e2021EA002001. https://doi.org/10.1029/2021EA002001

Jacob S, Shay L, Mariano A, Black P (2000) The 3D oceanic mixed layer response to Hurricane Gilbert. J Phys Oceanogr 30:1407–1429. https://doi.org/10.1175/1520-0485(2000)030<1407:TOMLRT>2.0.CO;2

Jaimes B, Shay L (2010) Near-inertial wave wake of Hurricanes Katrina and Rita over Mesoscale Oceanic Eddies. J Phys Oceanogr 40:1320–1337. https://doi.org/10.1175/2010JPO4309.1

Jan S, Chern C, Wang J, Chiou M (2012) Generation and propagation of baroclinic tides modified by the Kuroshio in the Luzon Strait. J Geophys Res: Oceans 117(C2). https://doi.org/10.1029/2011JC007229

Jelesnianski CP (1965) A numerical calculation of storm tides induced by a tropical storm impinging on a continental shelf. Mon Weather Rev 93(6):343–358. https://doi.org/10.1175/1520-0493(1993)093%3C0343:ANCOS%3E2.3.CO;2

Jiang G, Xu J, Wei J (2018) A deep learning algorithm of neural network for the parameterization of typhoon-ocean feedback in typhoon forecast models. Geophys Res Lett 45. https://doi.org/10.1002/2018GL077004

Jing Y, Sun J, Li R, Wu K, Yu Z, Lin P, Dong X, Babanin AV (2025a) The impact of wave-induced mixing on the simulation of the upper mixed layer in climate models. Ocean Model 197:102583. https://doi.org/10.1016/j.ocemod.2025.102583

Jing Y, Wu K, Li R, Yu Z (2025b) The effect of non-breaking wave mixing on ocean modeling in the South China Sea. J Mar Sci Eng 13(8):1548. https://doi.org/10.3390/jmse13081548

Jullien S, Menkes C, Marchesiello P, Jourdain N, Lengaigne M, Koch-Larrouy A et al (2012) Impact of tropical cyclones on the heat budget of the south pacific ocean. J Phys Oceanogr 42:1882–1906. https://doi.org/10.1175/JPO-D-11-0133.1

Kerry CG, Powell BS, Carter GS (2014a) The impact of subtidal circulation on internal tide generation and propagation in the Philippine Sea. J Phys Oceanogr 44:1386–1405. https://doi.org/10.1175/JPO-D-13-0142.1

Kerry CG, Powell BS, Carter GS (2014b) The impact of subtidal circulation on internal-tide-induced mixing in the Philippine Sea. J Phys Oceanogr 44:3209–3224. https://doi.org/10.1175/JPO-D-13-0249.1

Large WG, McWilliams JC, Doney SC (1994) Oceanic vertical mixing: a review and a model with a nonlocal boundary layer parameterization. Rev Geophys 32(4):363–403. https://doi.org/10.1029/94RG01872

Lin I, Wu C, Emanuel KA, Lee I, Wu C, Pun I (2005) The interaction of supertyphoon Maemi (2003) with a warm ocean Eddy. Mon Weather Rev 133(9):2635–2649. https://doi.org/10.1175/MWR3005.1

Lin I, Wu C, Pun I, Ko D (2008) Upper-ocean thermal structure and the western north pacific category 5 typhoons. Part I: Ocean Features and the Category 5 Typhoons' Intensification. Mon Weather Rev 136(9):3288–3306. https://doi.org/10.1175/2008MWR2277.1

Lin I, Pun I, Wu C (2009) Upper-ocean thermal structure and the western north pacific category 5 typhoons. Part II: Dependence on Translation Speed. Mon Weather Rev 137(11):3744–3757. https://doi.org/10.1175/2009MWR2713.1

Liu X, Wei J (2015) Understanding surface and subsurface temperature changes induced by tropical cyclones in the Kuroshio. Ocean Dynam 65(7):1017–1027. https://doi.org/10.1007/s10236-015-0851-9

Liu Y, Guan S, Lin II, Mei W, Jin F, Huang M, Zhang Y, Zhao W, Tian J (2023) Effect of storm size on sea surface cooling and tropical cyclone intensification in the western north pacific. J Clim 36(20):7277–7296. https://doi.org/10.1175/JCLI-D-22-0949.1

Ma Z, Fei J, Huang X, Cheng X (2018) Modulating effects of mesoscale oceanic Eddies on sea surface temperature response to tropical cyclones over the western north pacific. J Geophys Research: Atmos 123(1):367–379. https://doi.org/10.1002/2017JD027806

Mei W, Xie S (2016) Intensification of landfalling typhoons over the northwest Pacific since the late 1970s. Nat Geosci 9(10):753–757. https://doi.org/10.1038/ngeo2792

Nan F, Xue H, Chai F, Shi L, Shi M, Guo P (2011) Identification of different types of Kuroshio intrusion into the South China Sea. Ocean Dynam 61(9):1291–1304. https://doi.org/10.1007/s10236-011-0426-3

Nan F, Xue H, Yu F (2015) Kuroshio intrusion into the South China Sea: A review. Prog Oceanogr 137:314–333. https://doi.org/10.1016/j.pocean.2014.05.012

Nitani H (1975) Variation of the Kuroshio south of Japan. J Oceanogr Soc Jpn 31(4):154–173. https://doi.org/10.1007/BF02107107

Price JF (1981) Upper ocean response to a hurricane. J Phys Oceanogr 11(2):153–175. https://doi.org/10.1175/1520-0485(1981)011<0153:UORTAH>2.0.CO;2

Price JF, Sanford TB, Forristall GZ (1994) Forced stage response to a moving hurricane. J Phys Oceanogr 24(2):233–260. https://doi.org/10.1175/1520-0485(1994)024<0233:FSRTAM>2.0.CO;2

Qiao M, Cao A, Song J, Pan Y, He H (2022) Enhanced turbulent mixing in the upper ocean induced by super typhoon Goni (2015). Remote Sens 14(10):2300. https://doi.org/10.3390/rs14102300

Qu T, Mitsudera H, Yamagata T (2000) Intrusion of the North Pacific waters into the South China Sea. J Geophys Res: Oceans 105(C3):6415–6424. https://doi.org/10.1029/1999JC900323

Rimac A, Storch J, Eden C (2016) The total energy flux leaving the ocean's mixed layer. J Phys Oceanogr 46:1885–1900. https://doi.org/10.1175/JPO-D-15-0115.1

Schade LR, Emanuel KA (1999) The ocean's effect on the intensity of tropical cyclones: results from a simple coupled atmosphere–ocean model. J Atmos Sci 56(4):642–651. https://doi.org/10.1175/1520-6760469(1999)056<0642:TOSEOT>2.0.CO;2

Shay LK, Black PG, Mariano AJ, Hawkins JD, Elsberry RL (1992) Upper ocean response to Hurricane Gilbert. J Geophys Res: Oceans 97(C12):20227–20248. https://doi.org/10.1029/92JC01586

Shay LK, Goni GJ, Black PG (2000) Effects of a warm oceanic feature on hurricane Opal. Mon Weather Rev 128(5):1366–1383. https://doi.org/10.1175/1520-0493(2000)128<1366:EOAWOF>2.0.CO;2

Sprintall J, Tomczak M (1992) Evidence of the barrier layer in the surface layer of the tropics. J Geophys Res: Oceans 97(C5):7305–7316. https://doi.org/10.1029/92JC00407

Tan H, Cai R, Guo Z (2023) Increasing compound hazard of landfalling tropical cyclones in China during 1980–2020. Int J Climatol 43. https://doi.org/10.1002/joc.8296

Tory KJ, Dare RA (2015) Sea surface temperature thresholds for tropical cyclone formation. J Clim 28(20):8171–8183. https://doi.org/10.1175/JCLI-D-14-00637.1

Tseng C, Lin C, Chen S, Shyu C (2000) Temporal and spatial variations of sea surface temperature in the East China Sea. Cont Shelf Res 20(4):373–387. https://doi.org/10.1016/S0278-4343(99)00077-1

Vincent EM, Lengaigne M, Madec G, Vialard J, Samson G, Jourdain NC et al (2012a) Processes setting the characteristics of sea surface cooling induced by tropical cyclones. J Geophys Res: Oceans 117(C2). https://doi.org/10.1029/2011JC007396

Vincent EM, Lengaigne M, Vialard J, Madec G, Jourdain NC, Masson S (2012b) Assessing the oceanic control on the amplitude of sea surface cooling induced by tropical cyclones. J Geophys Res: Oceans 117(C5). https://doi.org/10.1029/2011JC007705

Watanabe M, Hibiya T (2002) Global estimates of the wind-induced energy flux to inertial motions in the surface mixed layer. Geophys Res Lett 29(8):61–64. https://doi.org/10.1029/2001GL014422

Wei J, Liu X, Wang D (2014) Dynamic and thermal responses of the Kuroshio to typhoon Megi (2004). Geophys Res Lett 41(23):8495–8502. https://doi.org/10.1002/2014GL061706

Wei J, Jiang G, Liu X (2017) Parameterization of typhoon-induced ocean cooling using temperature equation and machine learning algorithms: an example of typhoon Soulik (2013). Ocean Dynam 67(9):1179–1193. https://doi.org/10.1007/s10236-017-1082-z

Wu C, Lee C, Lin I (2007) The effect of the ocean Eddy on tropical cyclone intensity. J Atmos Sci 64(10):3562–3578. https://doi.org/10.1175/JAS4051.1

Wu C, Chang Y, Oey L, Chang CWJ, Hsin Y (2008) Air-sea interaction between tropical cyclone Nari and Kuroshio. Geophys Res Lett 35(12). https://doi.org/10.1029/2008GL033942

Xu X, Shen Z, Li J, Wang S (2020) The spatio-temporal characteristics of tropical cyclones hazard in the maritime silk road. J Geo-Information Sci 22(12):2383–2392

Xu Z, Wang Y, Liu Z, McWilliams JC, Gan J (2021) Insight into the dynamics of the radiating internal tide associated with the Kuroshio Current. J Geophys Res Oceans 126:e2020JC017018. https://doi.org/10.1029/2020JC017018

Yu Y, Dong C, Shan H, Zou B (2020) Statistical analysis of intensity variations in tropical cyclones in the East China Sea passing over the Kuroshio. J Oceanol Limnol 38(6):1632–1639. https://doi.org/10.1007/s00343-019-9069-x

Zhang H (2023) Modulation of upper ocean vertical temperature structure and heat content by a fast-moving tropical cyclone. J Phys Oceanogr 53(2):493–508. https://doi.org/10.1175/JPO-D-22-0132.1

Zhang H, Chen D, Zhou L, Liu X, Ding T, Zhou B (2016) Upper ocean response to typhoon Kalmaegi (2014). J Geophys Res: Oceans 121(8):6520–6535. https://doi.org/10.1002/2016JC012064

Zhang H, He H, Zhang W, Tian D (2021) Upper ocean response to tropical cyclones: a review. Geosci Lett 8:1. https://doi.org/10.1186/s40562-020-00170-8

Zhang W, Zhang J, Liu Q, Sun J, Li R, Guan C (2023b) Effects of surface wave-induced mixing and wave-affected exchange coefficients on tropical cyclones. Remote Sens 15(6):1594. https://doi.org/10.3390/rs15061594

Zhang W, Li R, Zhu D, Zhao D, Guan C (2023a) An investigation of impacts of surface waves-induced mixing on the upper ocean under typhoon Megi (2010). Remote Sens 15(7):1862. https://doi.org/10.3390/rs15071862

Zheng Z, Ho C, Zheng Q, Lo Y, Kuo N, Gopalakrishnan G (2010) Effects of preexisting cyclonic eddies on upper ocean responses to Category 5 typhoons in the western North Pacific. J Geophys Res: Oceans 115(C9). https://doi.org/10.1029/2009JC005562

Zhu T, Zhang D (2006) The impact of the storm-induced SST cooling on hurricane intensity. Adv Atmos Sci 23(1):14–22. https://doi.org/10.1007/s00376-006-0002-9

Publisher's Note Springer Nature remains neutral with regard to jurisdictional claims in published maps and institutional affiliations.